



Power Electronic Systems
Laboratory

© 2011 IEEE

IEEE Transactions on Dielectrics and Electrical Insulation, Vol. 18, No. 4, pp. 1171-1180, August 2011.

Design Procedure for Compact Pulse Transformers with Rectangular Pulse Shape and Fast Rise Times

D. Bortis
G. Ortiz
J.W. Kolar
J. Biela

This material is posted here with permission of the IEEE. Such permission of the IEEE does not in any way imply IEEE endorsement of any of ETH Zurich's products or services. Internal or personal use of this material is permitted. However, permission to reprint/republish this material for advertising or promotional purposes or for creating new collective works for resale or redistribution must be obtained from the IEEE by writing to pubs-permissions@ieee.org. By choosing to view this document, you agree to all provisions of the copyright laws protecting it.



Eidgenössische Technische Hochschule Zürich
Swiss Federal Institute of Technology Zurich

Design Procedure for Compact Pulse Transformers with Rectangular Pulse Shape and Fast Rise Times

D. Bortis, G. Ortiz, J.W. Kolar

Power Electronic Systems Laboratory, ETH Zurich, Switzerland

and J. Biela

Laboratory for High Power Electronic Systems, ETH Zurich, Switzerland

ABSTRACT

Microseconds range pulse modulators based on solid state technology often utilize a pulse transformer, since it could offer an inherent current balancing for parallel connected switches and with the turns ratio the modulator design could be adapted to the available semiconductor switch technology. In many applications as e.g. radar systems, linear accelerators or klystron/magnetron modulators a rectangular pulse shape with a fast rise time and a as small as possible overshoot is required. In reality, however, parasitic elements of the pulse transformer as leakage inductance and capacitances limit the achievable rise time and result in overshoot. Thus, the design of the pulse transformer is crucial for the modulator performance. In this paper, a step by step design procedure of a pulse transformer for rectangular pulse shape with fast rise time is presented. Different transformer topologies are compared with respect of the parasitic elements, which are then calculated analytically depending on the mechanical dimensions of the transformer. Additionally, the influence of the core material, the limited switching speed of semiconductors and the nonlinear impedance characteristic of a klystron are analyzed.

Index Terms - Pulse transformer, rise time, transformer topology, transformer design, solid state modulator.

1 INTRODUCTION

IN many application areas, the required output power level of test facilities in laboratories or in industry is rising and in more and more applications solid state modulators deploying for example IGBT modules, with a constantly increasing power handling capability, are utilized. In contrast to the spark gap switches, which can only be turned-on and have a limited life time and switching frequency, available fast semiconductor switches have a limited power handling capability, so that a parallel and/or series connection of the switches is required. The parallel connection of the semiconductors basically offers a more robust design due to the better capability of the switches to handle over-currents compared to over-voltages. In [1] it has been shown, that a modulator based on pulse transformer is the most suitable topology for pulses in the μs -range, since it could offer an inherent current balancing in parallel connected power semiconductors. Additionally, the turn ratio of the pulse transformer offers a degree of freedom that allows adapting the modulator design to the current and voltage ratings of available switch technology.

In applications like radar systems, linear accelerators or klystron and magnetron modulators, where a nearly rectangular pulse shape is needed, also the requirements with respect to rise times, overshoot or voltage droop are high. In Figure 1a the schematic waveform of a typical power modulator's output voltage and in b) a power modulator with the specifications given in Table 1 are shown. Since the transformer parasitic limit the achievable rise time and define the resulting overshoot, the design of the transformer is crucial. On the one hand, due to non-ideal material properties like the limited permeability ($\mu \neq \infty$) or the limited maximum flux density B_{max} of the core material, the maximum voltage-time-product respectively the minimum cut-off frequency f_u of the pulse transformer is defined.

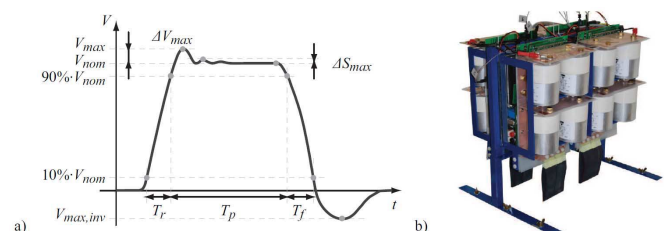


Figure 1. a) Typical pulse waveform; b) 20 MW pulse modulator.

Table 1. Specification of the 20 MW, 5 μ s pulse modulator.

DC Link Voltage V_{in}	1000V
Output Voltage V_{out}	200kV
Pulse Duration T_p	5 μ s
Output Power P_{out}	20MW
Rise Time T_r	< 500ns
Overshoot ΔV_{max}	< 3%
Turns ratio	1:170

On the other hand, in transformers no ideal magnetic coupling between windings can be achieved, which results in a certain leakage inductance L_σ . Additionally, parasitic capacitances of the transformer define the transient voltage distribution and result in combination with L_σ in an upper cut-off frequency f_o of the transformer. Often the parasitic capacitances are summarized in one single lumped capacitor C_d as will be shown later.

The output voltage with an almost rectangular pulse shape, however, exhibits a wide frequency spectrum. In order to transfer the voltage pulse with a minimum pulse distortion, especially during the rise time, a maximum bandwidth has to be achieved, which means that the mentioned parasitic of the transformer must be minimized.

Consequently, the pulse transformer is one of the key components of pulse modulators, which mainly defines the achievable rise time T_r and overshoot ΔV_{max} of the output voltage pulse.

In this paper, a general step by step design procedure of a pulse transformer is presented. In section 2 the influence of the parasitic elements L_σ and C_d is analyzed with a standardized pulse transformer model. During the rise time this model can be simplified, which allows to derive basic design equations concerning rise time and overshoot of the pulse transformer. Based on this, in section 3 different transformer topologies are compared with respect to the fastest achievable rise time. In order to define the mechanical dimensions, the leakage inductance L_σ and the capacitance C_d are calculated analytically in section 4. In order to achieve faster rise time, transformers with multiple cores can be used, as described in section 5. In section 6 the influence of the core material properties like permeability μ , maximum flux density B and the core losses during pulse excitation is evaluated based on experimental results.

In section 7 the influence of the limited switching speed of semiconductors and the nonlinear impedance characteristic of a klystron is evaluated. Experimental results of the built pulse modulator are shown in section 8.

2 PULSE TRANSFORMER'S EQUIVALENT CIRCUIT

In literature numerous electrical equivalent circuits considering LF and HF properties of pulse transformers have been proposed and IEEE standardized the equivalent circuit of pulse transformers [3] as shown in Figure 2a. In order to simplify the analysis of the transient behavior for operation with rectangular pulse voltages, the standardized equivalent circuit can be reduced to the equivalent circuit

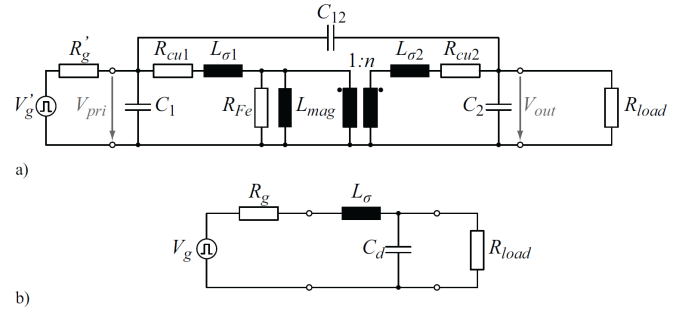


Figure 2. a) IEEE standardized equivalent circuit of a pulse transformer and b) simplified equivalent circuit during the leading edge.

shown in Figure 2b during the leading edge if $n \gg 1$ [4]. There, all impedances and the input voltage V_g are transferred to the secondary and, hence, the ideal transformer can be neglected. If nothing mentioned, in this paper, also all measured impedances are referred to the secondary. Since the pulse rise time T_r is in the range of some 100 ns and there is - due to very small voltage-time-product - no excitation of the core, the influence of the core material, i.e. R_{Fe} and L_{mag} , can be neglected during the rise time. Even if the core resistance R_{Fe} would be considered, it would not have an influence on the rise time, since it is connected in parallel to the load resistance, which in this case is $R_{load} = 1500 \Omega$ if referred to the secondary or $R_{load;pri} = 0.052 \Omega$ if referred to the primary. There, the load resistance R_{load} is much smaller than the resistance of the core material, which was calculated to $R_{Fe} \approx 4 \Omega$ on the primary.

Therefore, the rise time and the overshoot of the output voltage, are mainly defined by the leakage inductance L_σ and the capacitance C_d . Assuming an ideal step voltage at the primary, the output voltage $v_{out}(t)$ can be calculated with the Laplace-transform as described in [4].

$$v_{out}(t) = \frac{V_g R_{load}}{R_g + R_{load}} \left[1 - e^{-at} \left(\frac{a}{k} \sinh(kt) + \cosh(kt) \right) \right] \quad (1)$$

with $k^2 = a^2 - b$ and

$$2a = \frac{R_g}{L_\sigma} + \frac{1}{C_d R_{load}}, \quad b = \frac{1}{L_\sigma C_d} \left(1 + \frac{R_g}{R_{load}} \right)$$

where the damping coefficient σ of (1) is given by

$$\sigma = \frac{a}{\sqrt{b}} = \frac{C_d R_g R_{load} + L_\sigma}{2\sqrt{R_{load} L_\sigma C_d (R_g + R_{load})}}. \quad (2)$$

If it is assumed, that the output pulse shape is mainly defined by the transformer characteristics, the modulator's impedance R_g can be neglected. Thus, the damping coefficient σ considering only the influence of the transformer can be simplified to

$$\sigma = \frac{a}{\sqrt{b}} = \frac{1}{2R_{load}} \sqrt{\frac{L_\sigma}{C_d}} \quad (3)$$

As will be shown later, however, depending on the turns ratio of the pulse transformer, the pulse generator's parasitic inductance L_{gen} and capacitance C_{gen} - resulting from the dc-link capacitors, the switches and the interconnections - as well as the parasitic capacitance of the load C_d have to be considered for the calculation of the

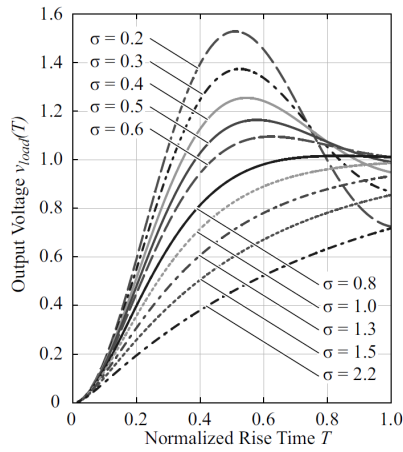


Figure 3. Transient behavior of the normalized output voltage for different damping coefficients σ .

overshoot and the rise time. For these cases, the input impedance should be changed from a resistance R_g to an impedance Z_g . If the step up ratio of the pulse transformer is high, the parasitic capacitance C_{gen} can be neglected, since it is transferred to the secondary, the capacitance is divided by n^2 , which is much smaller than the parasitic capacitance of the transformer C_d or the load C_{load} . In Figure 3 the transient behavior of the normalized output voltage during

$T = \frac{\sqrt{b}}{2\pi} t$ is illustrated. A decreasing damping coefficient σ results in a faster rise time T_r . Starting from $\sigma < 1$ a tradeoff between T_r and overshoot is found. Therefore, to achieve a minimum rise time T_r , the damping coefficient σ has to be selected as small as possible while the resulting overshoot has to be still below the maximum allowed value (Figure 1a and Table 1).

2.1 OVERSHOOT

Considering equation (3), σ depends on L_σ and C_d , i. e. on the pulse transformer's mechanical dimensions and on the load impedance R_{load} . In general, R_{load} , for example of a klystron, is defined by the application. Therefore, the pulse transformer's mechanical dimensions must be adjusted in order to fulfill the specifications of the pulse shape. Assuming a klystron load of $R_{load} = 1500 \Omega$, for a maximum overshoot of 3% a damping coefficient of $\sigma = 0.75$ is needed (equation (3)). Consequently, with a given R_{load} and σ , the ratio of leakage inductance L_σ and capacitance C_d is fixed by

$$2R_{load} \cdot \sigma = \sqrt{\frac{L_\sigma}{C_d}} \quad (4)$$

2.2 RISE TIME

In addition to the overshoot, the rise time T_r of the output voltage can be derived from equation (1). As shown in equation (5), T_r is proportional to the product of L_σ and C_d .

$$T = \frac{\sqrt{b}}{2\pi} t, \quad T_r = 2\pi T_{10\%-90\%} \sqrt{L_\sigma C_d} \quad (5)$$

Factor $T_{10\%-90\%}$ depends on the selected damping coefficient σ and equals the time in which the voltage

$v_{load}(t)$ rises from 10% to 90% (cf. Figure 3). For $\sigma = 0.75$ the factor is $T_{10\%-90\%} = 0.365$.

Since the rise time T_r is proportional to $L_\sigma \cdot C_d$, the parasitics have to be minimized in order to achieve the fastest possible rise time. For example, to keep the rise time below $T_r = 500$ ns, $L_\sigma \cdot C_d$ has to be smaller than 4.75×10^{-14} if $\sigma = 0.75$.

Since the load impedance is $R_{load} = 1500 \Omega$, the ratio of L_σ and C_d is fixed and the maximum values for the specifications in Table I are: $L_\sigma < 490 \mu\text{H}$, $C_d < 97$ pF.

2.3 DESIGN CRITERIA

In order to fulfill the requirements for the maximum overshoot and the maximum rise time, both a given ratio of L_σ to C_d and a maximum product of L_σ and C_d have to be guaranteed. In general, the pulse modulator connected to the transformer's primary as well as the load connected to the secondary winding have a certain inductance $L_{gen} /$ capacitance C_{load} , which also have to be considered. For the realized pulse generator a parasitic inductance of $L_{gen} = 260 \mu\text{H}$ was measured. Typical capacitance values of klystrons are in the range of $C_{load} = 40 - 120$ pF [18] for the considered application. This means that the leakage inductance and the distributed capacitance of the transformer must be small to meet the pulse specifications. Therefore, equations (4) and (5) have to be extended to

$$2R_{load} \cdot \sigma = \sqrt{\frac{L_\sigma + L_{gen}}{C_d + C_{load}}} \quad (6)$$

$$T_r = 2\pi T_{10\%-90\%} \sqrt{(L_\sigma + L_{gen})(C_d + C_{load})}$$

3 TRANSFORMER TOPOLOGY

The ratio of L_σ and C_d can be varied by the mechanical dimensions of the transformer, i.e. the distances, the heights and the lengths of the windings. The product of L_σ and C_d , however, is defined by the transformer topology and can be assumed to be approximately constant [4]. Therefore, first the transformer topology resulting in the smallest $L_\sigma C_d$ -product has to be selected. Afterwards, the mechanical dimensions must be calculated to achieve the needed $L_\sigma C_d$ -ratio.

In the following, the $L_\sigma C_d$ -product of three different transformer topologies is analyzed. The leakage inductance L_σ and the capacitance C_d are calculated with the energy stored in the magnetic & electric field.

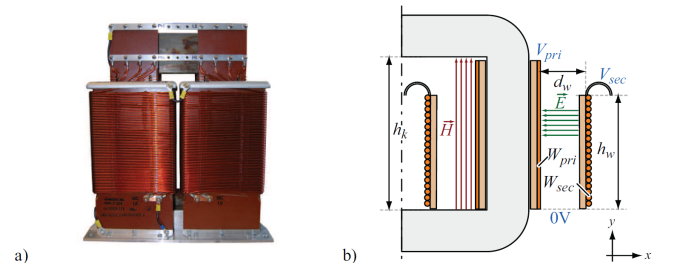


Figure 4. a) Picture of a pulse transformer with parallel winding and b) 2D drawing of one leg with simplified run of the magnetic and electric field lines.

$$E_{mag} = \frac{1}{2} \mu \int_V \vec{H}^2 dV \equiv \frac{1}{2} L_\sigma \cdot I_{pri}^2 \quad (7)$$

$$E_{elec} = \frac{1}{2} \varepsilon \int_V \vec{E}^2 dV \equiv \frac{1}{2} C_d \cdot V_{pri}^2 \quad (8)$$

To simplify the comparison, only the energies between the windings are considered. Finally, for the transformer topology with the smallest $L_\sigma C_d$ -product a more detailed calculation of the parasitic is presented.

3.1 PARALLEL WINDING

Due to the simple construction, the parallel winding topology is widely used. The primary and secondary are wound on two parallel bobbins, whose distance is defined by the required isolation. In Figure 4a picture and 2D drawing of the parallel winding are shown.

The leakage inductance is mainly defined by the volume and the magnetic field strength between the bobbins (equation (7)). According to Ampere's law and assuming an ideal core material ($\mu = \infty$), the magnetic field strength \vec{H} in the core window is given by the primary current times the number of turns $N_{pri} I_{pri}$ and the height of the core h_k .

$$|\vec{H}| = \frac{N_{pri} I_{pri}}{h_k} \quad (9)$$

Using equations (7) and (9), the stored magnetic energy E_{mag} between the windings W_{pri} and W_{sec} can be approximately calculated by

$$E_{mag} = \frac{1}{2} \mu (N_{pri} I_{pri})^2 \frac{l_w \cdot d_w}{h_k} = \frac{1}{2} L_\sigma I_{pri}^2, \quad (10)$$

and the resulting leakage inductance $L_{\sigma,parallel}$ is

$$L_{\sigma,parallel} = \mu \frac{N_{pri}^2 \cdot l_w \cdot d_w}{h_k}. \quad (11)$$

To calculate the capacitance C_d , a linear voltage distribution

$V_{pri}(y)$ and $V_{sec}(y)$ is assumed across the windings.

$$V_{pri}(y) = \frac{y}{h_w} V_{pri}; \quad V_{sec}(y) = \frac{y}{h_w} V_{sec} \quad (12)$$

Therewith, the voltage difference between the primary and secondary winding depending on the vertical position y is $\Delta V(y) = V_{sec}(y) - V_{pri}(y)$.

Due to the voltage difference between the windings W_{pri} and W_{sec} , the electric field lines run approximately horizontally (Figure 4b). Thus, the electric field $\vec{E}(y)$ depending on the y -position is

$$|\vec{E}(y)| = \frac{\Delta V(y)}{d_w} = \frac{V_{pri} \cdot (n-1) \cdot y}{h_w \cdot d_w} \approx \frac{V_{sec} \cdot y}{h_w \cdot d_w}. \quad (13)$$

Considering equation (8), the stored energy between the windings W_{pri} and W_{sec} and therewith the capacitance C_d are calculated.

$$\begin{aligned} E_{elec} &= \frac{1}{2} \varepsilon \int_0^{l_w} \int_0^{h_w} \int_0^{d_w} \left(\frac{V_{sec} \cdot y}{h_w \cdot d_w} \right)^2 dx dy dz \\ &= \frac{1}{6} \varepsilon V_{sec}^2 \cdot \left(\frac{l_w \cdot h_w}{d_w} \right) = \frac{1}{2} C_d \cdot V_{pri}^2 \end{aligned} \quad (14)$$

$$C_{d,parallel} = \frac{1}{3} \cdot \varepsilon \cdot \left(\frac{N_{sec}}{N_{pri}} \right)^2 \cdot \left(\frac{l_w \cdot h_w}{d_w} \right) \quad (15)$$

Finally, the $L_\sigma C_d$ -product of the transformer topology with parallel windings is

$$L_{\sigma,parallel} C_{d,parallel} = \frac{1}{3} \cdot \varepsilon \mu \frac{N_{sec}^2 \cdot l_w^2 \cdot h_w}{h_k}. \quad (16)$$

3.2 CONE WINDING

Since the distance between the windings of the transformer with parallel winding is constant but the voltage is increasing linearly in y -direction, the electric field between the windings also increases linearly. In order to achieve a constant electric field $\vec{E}(y)$ the distance between the windings d_w has to be linearly decreased for smaller voltage differences, which results in a cone winding [4], [19] as shown in Figure 5.

Compared to the parallel winding, the volume between the windings and therefore also the leakage inductance L_σ can be reduced by a factor of two. However, due to the smaller distance between the windings C_d is increases.

To calculate the leakage inductance L_σ of the cone winding, again, a constant magnetic field in y -direction is assumed (Figure 5), which was confirmed by FEM-simulation as long as $d_w \ll h_w$.

Considering equation (7), the stored magnetic energy E_{mag} and the resulting leakage inductance $L_{\sigma,cone}$ are

$$E_{mag} = \frac{1}{4} \mu (N_{pri} I_{pri})^2 \frac{l_w \cdot d_w}{h_k} = \frac{1}{2} L_\sigma I_{pri}^2 \quad (17)$$

$$L_{\sigma,cone} = \frac{1}{2} \cdot \mu \frac{N_{pri}^2 \cdot l_w \cdot d_w}{h_k}. \quad (18)$$

Due to the linearly increasing distance $d_w(y)$ and the voltage distribution $\Delta V(y)$ in y -direction, the electric field \vec{E} between the winding is constant and runs approximately parallel to the x -direction (Figure 5b). Hence, the stored electric energy (equation (8)) for a cone winding and the capacitance C_d are

$$E_{elec} = \frac{1}{4} \varepsilon V_{sec}^2 \cdot \left(\frac{l_w \cdot h_w}{d_w} \right) = \frac{1}{2} C_d \cdot V_{pri}^2 \quad (19)$$

$$C_{d,cone} = \frac{1}{2} \cdot \varepsilon \cdot \left(\frac{N_{sec}}{N_{pri}} \right)^2 \cdot \left(\frac{l_w \cdot h_w}{d_w} \right) \quad (20)$$

Finally, the resulting $L_\sigma C_d$ -product of the cone winding is

$$L_{\sigma,cone} C_{d,cone} = \frac{1}{4} \cdot \varepsilon \mu \frac{N_{sec}^2 \cdot l_w^2 \cdot h_w}{h_k}. \quad (21)$$

Compared to the parallel winding, the $L_\sigma C_d$ -product can be reduced by 25%, which results in a rise time improvement of 13.4%.

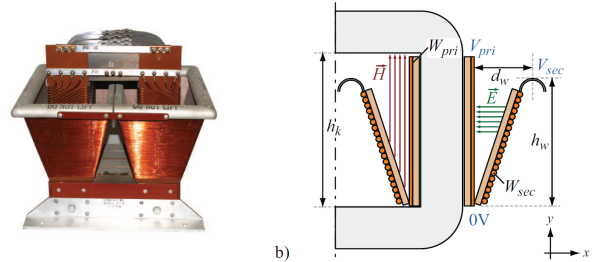


Figure 5. a) Picture of a pulse transformer with cone winding and b) 2D drawing of one leg with simplified run of the magnetic and electric field lines.

3.3 FOIL WINDING

Finally, for the primary W_{pri} and secondary W_{sec} foil windings are considered. The secondary is directly wound on the primary winding as shown in Figure 6. For the isolation of the turns a material with a low permittivity is used.

The thickness d_{iso} of the isolation can be kept small, since the voltage difference between two consecutive turns is just $V_{w,w} = V_{sec}/N_{sec}$. However, due to the increasing voltage difference between the turns and the core, the winding's height is linearly decreased from $h_{w,1}$ to $h_{w,2}$ (Figure 6b). The total thickness d_w of the winding is defined by the thickness of the isolation d_{iso} and the foil d_{cu} times the number of turns.

The leakage inductance L_σ of the foil winding is calculated again with the stored magnetic energy (equation (7)). Based on Ampere's law, the magnetic field is gradually increasing with the number of turns n_L , since the enclosed amount of current is increasing gradually (Figure 6).

$$\vec{H}(n_L) = \frac{n_L I_{sec}}{h_k} \quad (22)$$

The total magnetic energy is the sum of all energies between two consecutive turns, which is

$$\begin{aligned} E_{mag} &= \frac{1}{2} \mu V(n_L) \sum_{n_L=1}^{N_{sec}} \vec{H}(n_L)^2 = \frac{1}{2} \mu \frac{I_{sec}^2}{h_k^2} V(n_L) \sum_{n_L=1}^{N_{sec}} n_L^2 \\ &\approx \frac{1}{4} \mu (N_{pri} I_{pri})^2 \frac{l_w \cdot d_w}{h_k} = \frac{1}{2} L_\sigma I_{pri}^2. \end{aligned} \quad (23)$$

Thus, the resulting $L_{\sigma,foil}$ is

$$L_{\sigma,foil} = \frac{1}{2} \cdot \mu \frac{N_{pri}^2 \cdot l_w \cdot d_w}{h_k}. \quad (24)$$

Capacitance C_d can be calculated as a series connection of parallel plate capacitors between consecutive turns $C_{w,w}$. The distance of the plates equals d_{iso} , which can be expressed by the total winding thickness.

$$d_{iso} = \frac{d_w}{(k+1) \cdot N_{sec}} \quad \text{where } k = d_{cu}/d_{iso} \quad (25)$$

Assuming a constant winding height $h_w = (h_{w,1} + h_{w,2})/2$, the capacitance C_d for the foil winding results in

$$C_{d,foil} = (k+1) \cdot \varepsilon \cdot \left(\frac{N_{sec}}{N_{pri}} \right)^2 \left(\frac{h_w \cdot l_w}{d_w} \right) \quad (26)$$

and the $L_\sigma C_d$ -product is

$$L_{\sigma,foil} C_{d,foil} = \frac{k+1}{2} \cdot \varepsilon \mu \frac{N_{sec}^2 \cdot l_w^2 \cdot h_w}{h_k}. \quad (27)$$

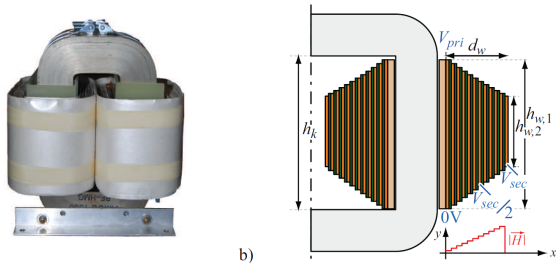


Figure 6. a) Picture of a pulse transformer with foil winding and b) 2D drawing of one leg.

Considering only the stored magnetic and electric energy between the windings W_{pri} and W_{sec} , the smallest $L_\sigma C_d$ -product and therefore the fastest T_r can be achieved for the transformer with a cone winding. Since the considered volume contains the major share of the magnetic and electric energy, the calculated $L_\sigma C_d$ -product is a reliable indicator for selecting the best transformer topology.

4 PARASITICS CALCULATION

In a next step, also the magnetic and electric fields between the winding and the core as well as the electric fields between the windings and the enclosing wall of a tank are considered in order to obtain a more precise model for designing the transformer. For example, in Figure 7a, the resulting electric field \vec{E} for a transformer placed in a tank is shown.

As it was proposed in [4], in Figure 8a a measured and a calculated waveform considering only the energy stored between the windings are shown. It clearly indicates the mismatch between measurement and simplified calculation of the parasitics. Since only the electric energy between the windings is considered, C_d is too small and results in a too small overshoot predicted by the transformer model. Therefore, a more detailed calculation procedure, which considers all stored electric and magnetic energies, is needed.

4.1 DISTRIBUTED CAPACITANCE

To improve parasitics calculation the energy outside the windings is considered in the following. As shown in Figure 7b, the space around the transformer is divided into six relevant regions R_1 to R_6 . With geometric approximations, the stored energy in each region can then be calculated analytically. In [2] the detailed calculation of the distributed capacitances depending on the mechanical dimensions of the transformer is investigated. There, the calculated values have been compared with measured and simulated impedance values determined by FEM-simulation. The output voltage predicted with the improved model is shown in Figure 8b.

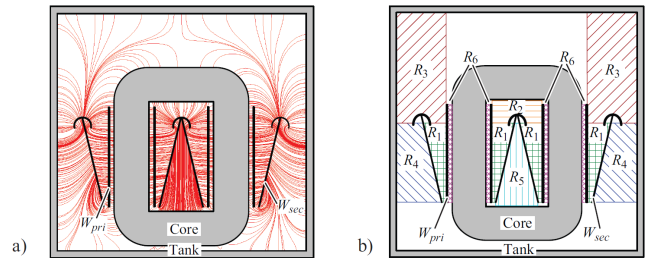


Figure 7. a) Electric field \vec{E} of a transformer with cone winding in a tank. b) Six relevant regions for calculating capacitance C_d .

Table 2. Relative stored electric energy of each region $R1/R6$ with and without tank.

Region	R_1	R_2	R_3	R_4	R_5	R_6
With tank	22.6%	6.4%	44.4%	25.2%	0.6%	0.8%
Without tank	33.9%	9.6%	44.3%	10.1%	0.9%	1.2%

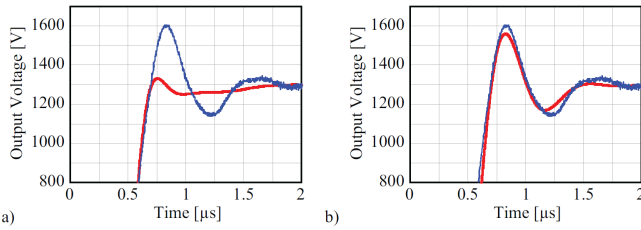


Figure 8. Comparison of measured and calculated output voltage if a) only the energy between the winding and b) the energy in all regions is considered.

The energies in all regions R_1 - R_6 have to be calculated and with the total electric energy, C_d can be determined. As an example, in Table 2 the relative stored electric energy in each region for a transformer with cone winding with and without tank is listed.

There, it is assumed, that the distance between the upper end of the secondary winding and the tank is the same as the distance between primary and secondary, which is d_w .

Table 2 clearly shows that only about a quarter of the total electric energy is stored between the windings. Considering only R_1 , in practice, the design of the transformer would result in a too large overshoot, since the real distributed capacitance would be much larger than the calculated one.

4.2 LEAKAGE INDUCTANCE

Compared to the capacitance C_d , the calculation L_σ is more challenging, since there no simple division into subregions is possible.

To precisely calculate the stored magnetic energy, FEM simulations are used. In Figure 9 the energy density for a pulse transformer with cone winding is illustrated.

The simulation shows, that the major part of the magnetic energy is concentrated in the region between the windings and the magnetic field $|\vec{H}|$ is almost constant. Therefore, the simple calculation of L_σ in section 2 (equation (18)) already matches the real leakage inductance well. Compared to FEM simulation the relative error of the simple equation is in the range of 10-20% if $d_w \ll h_w$.

5 INTERCONNECTION OF PULSE TRANSFORMERS

Instead of one pulse transformer also several pulse transformers could be used, which are connected either in

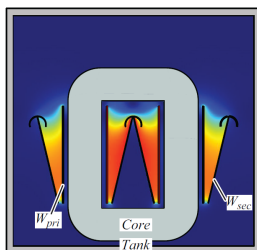


Figure 9. Magnetic energy density for a pulse transformer with cone winding.

parallel/parallel, parallel/series, series/parallel or in series/parallel on the primary/secondary.

5.1 PARALLEL OR SERIES CONNECTION OF PULSE TRANSFORMERS

In Figure 10 the equivalent circuits of two parallel a) and two series b) connected identical pulse transformers are shown. There, also an interconnection of an arbitrary number of transformers would be possible. However, considering Figure 10, it is directly obvious that no reduction of the $L_\sigma C_d$ -product and the rise time T_r can be achieved by such an interconnection.

With the parallel connection of the secondaries, for example, the total leakage inductance L_σ is halve as big as with one transformer, whereas the total capacitance C_d doubles. The only advantages are the reduction of winding resistance and the more flexible design if several switches have to be connected to the pulse transformer.

Additionally, the transformer geometry will change, since the ratio of L_σ to C_d is changed by a factor of four. However, the costs and the losses of the core material will increase.

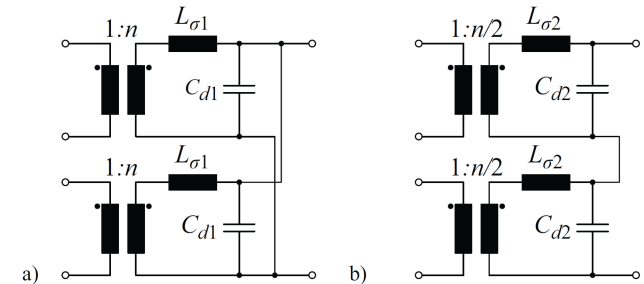


Figure 10. Equivalent circuit of two identical pulse transformers, which are a) connected in parallel and b) connected in series.

5.2 MULTIPLE CORE / MATRIX TRANSFORMER

In contrast to parallel or series connection of multiple pulse transformers a reduction of the $L_\sigma C_d$ -product and the rise time T_r can be achieved if a pulse transformer with multiple cores is used, which are usually called matrix transformer, fractional turn transformer, split-core transformer or voltage adder [1, 6-11].

In Figure 11a the top view of two in series connected pulse transformers is shown, where $N_{pri} = 1$ and $N_{sec} = n=2$. As mentioned before, by connecting transformers in series or parallel no improvements regarding T_r can be achieved. However, instead of connecting the secondaries in series, both secondaries can be combined to one secondary which

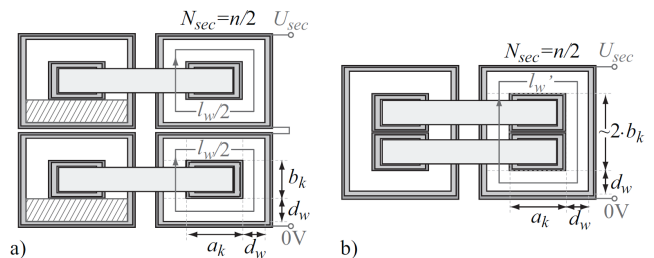


Figure 11. Top view of a) series connected pulse transformers with $N_{sec} = n/2$ and winding length l_w and b) pulse transformer with two cores and reduced winding length l_w' .

encloses both cores, whereas some volume between the primary and secondary winding is saved (Figure 11b). The saved volume directly results in a reduced leakage inductance and distributed capacitance compared to the series connection of the standard transformers. For this transformer configuration the conversion ratio between the primary and secondary voltage is not only defined by the turns ratio n but also by the ratio of enclosed core areas A^{pri} and A_{sec} (equation (28)) [1].

$$\frac{V_{out}}{V_{in}} = \frac{N_{sec}}{N_{pri}} \cdot \frac{A_{sec}}{A_{pri}} \quad (28)$$

Since T_r is proportional to the winding length, the reduction of T_r can directly be calculated by the winding length's reduction.

$$l_w = 4 \cdot a_k + 4 \cdot b_k + 8 \cdot d_w$$

$$l'_w = 2 \cdot a_k + 4 \cdot b_k + 4 \cdot d_w \quad (29)$$

For the considered transformer the distance between primary and secondary is $d_w = 2.5$ cm and the core dimensions are $a_k = b_k = 5$ cm. Consequently, the winding length of the transformer was reduced from $l_w = 60$ cm to $l'_w = 40$ cm, which results in a T_r reduction of 33%.

In order to further reduce the rise time, additional cores could be used. However, the relative improvement decreases for increasing number of cores, whereas the costs for the core material increase.

6 CORE MATERIAL

Beside the winding topology, the selection of the core material is crucial, since non-ideal material properties like the limited permeability ($\mu \neq \infty$) or the limited B_{max} directly influence the achievable bandwidth and therefore the performance of the pulse transformer.

With a higher B_{max} , for example, the core cross section can be reduce, which results in smaller parasitics and therefore in faster rise times.

In Table 3 different core materials are listed [12]. There, with cobalt-iron alloys the highest flux densities can be achieved. Due the high prices, however, this material is mainly used in military or aerospace applications [13]. Iron and silicon-iron alloys are the cheapest core material, where

Table 3. Core materials and maximum flux density B_{max} [12].

CoFe (35%-65%)	2.43T
Fe	2.16T
SiFe (3%)	2T
Ni (75%)	0.6T
NiFe (50%-50%)	1.6T

Table 4. Analyzed core materials and manufacturers.

Finemet FT3-M (nanocrystalline) (18 μ m)	Hitachi
2605SA1 (amorphous)(25 μ m)	Metglas
SiFe alloy 3% (50 μ m)	e.g. Magnetics

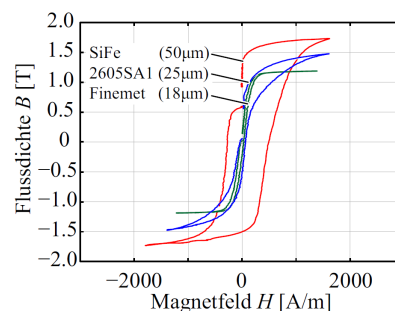


Figure 12. Measured hysteresis curve with flux excitation to B_{max} .

the second highest flux density can be achieved. Unfortunately, these materials also have the highest core losses. Nickel and nickel-iron alloys result in the lowest core losses, which only can be achieved with amorphous and nanocrystalline materials [14].

For the considered pulse transformer only silicon-iron alloys, due to the high flux density and the low cost, as well as iron based amorphous and nanocrystalline core materials, due to the low losses, were analyzed (Table 4).

The measured hysteresis curves of the materials listed in Table 4 are shown in Figure 12 for a pulse excitation of 5 μ s. There, the core was premagnetized with a passive premagnetization circuit. Due to premagnetization of the transformer core - either with passive [15] or active circuits [16, 17] - the total flux swing during one pulse can be doubled. Consequently, with a premagnetization circuit for the pulse transformer only half the core cross section is required. This further results in shorter winding lengths (lower copper losses), in a smaller volume between the windings (lower leakage inductance and distributed capacitance) and finally in a reduced rise time. Due to the higher core losses, however, a proper design concerning maximum allowable flux swing has to be done. On the one hand the core losses increase since the flux swing is doubled; on the other hand the core losses are reduced since the core volume is halved. In total the core losses will increase due to the nonlinear relation between flux density and core losses. With silicon-iron a maximum flux density

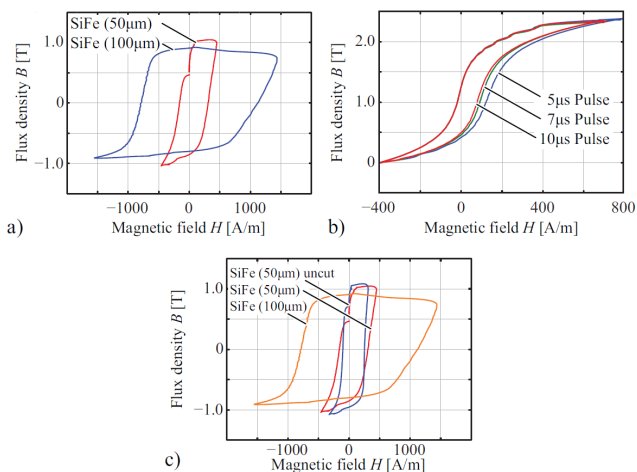


Figure 13. Measured hysteresis curve of a) SiFe alloy with tape thicknesses of 50 μ m and 100 μ m and b) of 2605SA1 for different pulse durations of 5 μ s, 7 μ s and 10 μ s and c) influence of a cut in the core material on the hysteresis curve.

of $B_{sat} = 1.73T$ was achieved. Since the flux density defines the needed core cross section, compared to Finemet (1.18T) and 2605SA1 (1.47T) the core cross section of silicon-iron would be 46% respectively 17% smaller.

As already mentioned, due to the core losses - which are given by the area of the hysteresis curve - the flux excitation is usually much below the maximum flux density, which mainly depends on the pulse repetition rate and the allowable average core losses. As shown in Figure 12, SiFe has the largest and Finemet the smallest areas in the hysteresis curve. Therefore, for a proper selection of the core material beside B_{max} also the core losses have to be considered, since the efficiency can be increased and the cooling effort is reduced. However, it has to be mentioned that the core losses are not only defined by the selected material. As shown in Figure 13a, for example, the thickness of the metal tape used in tape wound cores or the pulse duration, as shown in Figure 13b, can strongly influence the core losses. In addition a cut in the core material, which has been done due to fabrication reasons of the pulse transformer, leads to a lower permeability, to a slightly larger hysteresis loop and consequently to higher core losses, as shown in Figure 13c. Therefore, in order to compare different core materials regarding core losses, the same conditions must be applied.

7 DESIGN PROCEDURE

As described in section II, T_r and the overshoot mainly depend on the ratio and the product of the total series inductance $L_{gen} + L_\sigma$ and the total capacitance $C_d + C_{load}$. There, the basic equations were derived based on an ideal rectangular input voltage and a resistive load. However, in reality, the switching times of power semiconductors like IGBT modules are in best case in the range of some 100 ns. Consequently, due to the reduced voltage slope of the input voltage also the rise time is increased, which results in a decreased overshoot.

In addition, the impedance characteristic of the klystron is nonlinear and decreases with voltage, which also leads to an additional damping. Therefore, the influence of these effects has to be analyzed, since the design criteria like the needed damping coefficient σ and the resulting T_r are changed.

6.1 INFLUENCE OF POWER SEMICONDUCTOR SWITCHING SPEED

To calculate the influence of the limited switching speed of the power semiconductor on T_r and the overshoot, the real input voltage is approximated by a trapezoidal voltage. According to section 2, the output voltage $v(t)$ is again calculated with the Laplace-transform and the equivalent circuit shown in Figure 2b.

In Figure 14a the resulting transient responses of the output voltage for different turn-on times T_{on} respectively voltage slopes of $T_{on} = 0$ ns, $T_{on} = 120$ ns, $T_{on} = 300$ ns and $T_{on} = 500$ ns and for $L_\sigma = 250$ $\mu\text{H}/C_d = 200$ pF are

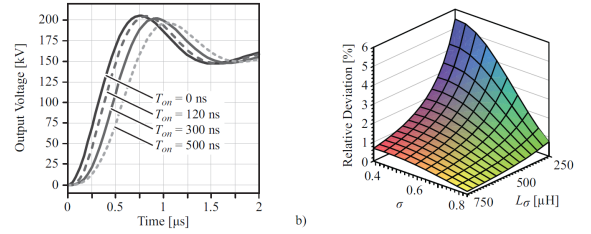


Figure 14. a) Transient responses for different turn-on times T_{on} of the semiconductor and b) relative difference in overshoot for a turn-on time of $T_{on} = 300$ ns.

illustrated. Due to the increased T_{ons} , T_r is increased whereas the overshoot is decreased.

There, the relative reduction of the overshoot is not only depending on the switching speed T_{on} and the ratio of L_σ and C_d but also on the absolute values of L_σ and C_d (Figure 14b).

As shown in Figure 14a, for T_{on} in the range of ≈ 100 ns the influence of the limited switching speed can be neglected, which in the worst case results in a relative overshoot reduction of less than 0.4%. However, for switching times above $T_{on} \approx 300$ ns the limited switching speed must be considered (Figure 14). It has to be mentioned, that the actual turn on characteristic (forward voltage drop vs. time) of IGBTs tends to reduce the overshoot.

6.2 INFLUENCE OF NONLINEAR KLYSTRON IMPEDANCE

In general, for the design and the initial operation of the power modulator, the klystron is substituted by an equivalent resistive load R_{load} . On the one hand, this substitution simplifies the design of the system and on the other hand, the klystron is an expensive and sensitive amplifier, which can be easily damaged during initial tests. However, for the design of the power modulator, especially of the pulse transformer, the nonlinear impedance characteristic of the klystron has to be considered. As described in [20, 21], the klystron results in a higher damping compared to the equivalent resistance, whereas during the rising edge the damping coefficient changes from 0.6 to 0.9 due to the nonlinear impedance. Therefore, with a klystron load a smaller damping coefficient σ is needed compared to the equivalent resistive load.

According to [20], the klystron's impedance can be modeled by

$$I_k = k \cdot V_k^{2/3} \quad (30)$$

where k is the perveance of the klystron.

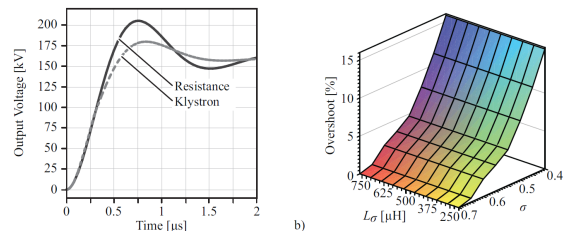


Figure 15. a) Comparison of the transient responses for a klystron load and a resistive load. b) Relative difference in overshoot for a turn-on time of $T_{on} = 300$ ns.

Considering equation (30), the klystron current I_k decreases more than linear with increasing klystron voltage, which results in a decreasing resistance for higher voltages and therefore in a decreasing overshoot compared to a linear load. The resulting transient responses for a klystron load and a resistive load are shown in Figure 15a assuming $L_\sigma = 250 \mu\text{H}$ and $C_d = 200 \text{ pF}$. The klystron leads to a significantly reduced overshoot compared to a resistive load.

Since the overshoot of 3% is specified for a klystron load, for the equivalent resistive load the pulse transformer has to be designed with a much higher overshoot, which is in this case 11%. Compared to the calculation in section II, the damping coefficient has to be decreased from $\sigma = 0.75$ to $\sigma = 0.58$.

In contrast to the limited switching speed, the influence of the klystron load on the overshoot does not depend on the absolute values of L_σ and C_d but only depends on the damping coefficient σ , as shown in Figure 15b.

8 EXPERIMENTAL RESULTS

In Figure 16 the measured output voltage and the built pulse transformer for a 20 MW power modulator with a klystron load is shown.

The measured T_r is below 500 ns and the overshoot with resistive load is 10.4%. This matches well with the 11% overshoot calculated for a passive load. Due to the larger damping, with the klystron the resulting overshoot will be below 3%.

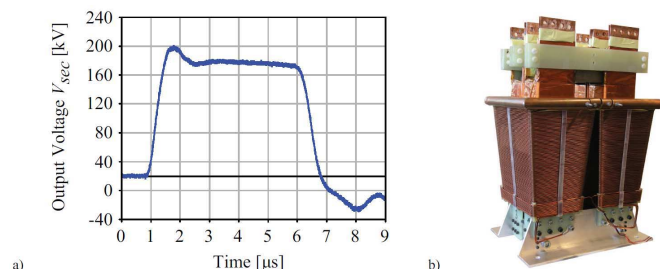


Figure 16. a) Measured output voltage waveform and b) designed pulse transformer for the specifications given in Figure 1.

9 CONCLUSION

In this paper, a step-by-step design procedure of a pulse transformer for rectangular pulse shapes and a fast rise time is presented.

Based on the transformer model, it could be seen that the rise time of transformers is proportional to the product of the leakage inductance L_σ and the parasitic output capacitance C_d of the pulse transformer.

This product is calculated for three different transformer topologies: parallel, cone and foil winding concepts and it is shown that with a cone winding the fastest rise time can be achieved.

The resulting overshoot is defined by the $L_\sigma C_d$ -ratio. For the calculation of these parasitics an improved calculation procedure is proposed and validated by measurements.

In addition to the transformer parasitics, also the nonlinear impedance characteristic of a klystron and the limited switching speed of semiconductors have to be considered in the design of the transformer as it is shown in the paper and validated by measurement results.

REFERENCES

- [1] D. Bortis, J. Biela and J.W. Kolar, "Transient Behaviour of Solid State Modulator with Split Core Transformer", IEEE Intern. Pulsed Power Conf. (PPC), Washington DC, USA, pp. 1396 – 1401, 2009.
- [2] J. Biela, D. Bortis and J.W. Kolar, "Modeling of Pulse Transformers with Parallel- and Non-Parallel-Plate Windings for Power Modulators", IEEE Trans. Dielectr. Electr. Insul., Vol. 14, pp.1016–1024, 2007.
- [3] The Institute of Electrical and Electronics Engineers, "IEEE Standards for Pulse Transformers", ANSI/IEEE Std 390-1987, 1987.
- [4] N. G. Glasoe and J. V. Lebacqz, *Pulse Generators*, MIT Radiation Laboratory Series, Vol. 5, McGraw-Hill Book, New York, 1948.
- [5] M. Akemoto, S. Gold, A. Krasnykh and R. Koontz, "Pulse Transformer R&D for NLC Klystron Pulse Modulator", IEEE 11th Pulsed Power Conf., Baltimore MA, USA, Vol. 1, pp. 724-729, 1997.
- [6] W. Crewson, M. Lindholm and D.K. Woodburn, "A New Solid State High Power Pulsed Modulator", United States Patent, Patent No. 5905646, 1999.
- [7] W. Crewson, M. Lindholm and D. K. Woodburn, "Power Modulator", Scanditronix Medical AB, Patent US 5905646A, May 1999.
- [8] W. Crewson and D. K. Woodburn, "Power Modulator Having at Least One Pulse Generating Module; Multiple Cores; And Primary Windings Parallel-Connected such that each Pulse Generating Module Drives all Cores", Patent US 2003/0128554 A1, 2003.
- [9] M. Akemoto, Y. H. Chin and Y. Sakamoto, "High-Power Klystron Modulator Using Solid-State IGBT Modules", 2nd Asian Particle Accelerator Conf., Beijing, China, pp. TUP001, 2001.
- [10] E. Herbert, "Flat Matrix Transformer", Patent US 4665357, May 1987.
- [11] E. Herbert, "High Frequency Matrix Transformer", Patent US 4845606, 1989.
- [12] R. Böll, *Weichmagnetische Werkstoffe*, Book, Wiley-VCH Verlag, Germany, Issue 4, 1990.
- [13] A. W. Molvik and A. Faltens, "Induction core alloys for heavy-ion inertial fusion-energy accelerators", Phys. Rev. Special Topics - Accelerators and Beams, Vol. 5, Issue 8, Paper No. 080401, 2002.
- [14] G. E. Fish, "Soft Magnetic Materials", Proceedings of IEEE, Vol. 78, Issue 6, Page(s): 947-972, Jun. 1990.
- [15] D. Bortis, J. Biela and J. W. Kolar, "Optimal Design of a DC Reset Circuit for Pulse Transformers", IEEE 20th Applied Power Electronics Conf. (APEC), Anaheim CA, USA, pp. 1171-1177, 2007.
- [16] J. Biela, D. Bortis and J.W. Kolar, "Reset Circuits with Energy Recovery for Solid State Modulators", IEEE Trans. Plasma Science, Vol. 36, Issue 5, pp. 2626-2631, 2008.
- [17] D. Bortis, J. Biela and J. W. Kolar, "Design and Control of an Active Reset Circuit for Pulse Transformers", IEEE Trans. Dielectrics and Electrical Insulation, Vol. 16, Issue 4, pp. 940-947, 2009.
- [18] J. S. Oh, M.H. Cho, W. Namkung, K. H. Chung, T. Shintake and H. Matsumoto, "Rise time analysis of pulsed klystron modulator for efficiency improvement of linear colliders", Nuclear Instruments and Methods in Physics Research Section A, Vol. 443, No. 2-3, pp. 223-230, 2000.
- [19] H. W. Lord, "Pulse Transformers", IEEE Trans. Magnetics, Vol. 7, pp. 17-28, 1971.
- [20] G. Caryotakis, *High Power Klystrons: Theory and Practice at the Stanford Linear Accelerator Center*, SLAC-PUB, 2004.
- [21] J. S. Oh, M. H. Cho, W. Namkung, T. Shintake, H. Matsumoto, K. Watanabe and H. Baba, "Efficiency Analysis of the first 111- MW C-Band Klystron-Modulator for Linear Collider", Particle Accelerator Conf. (PAC), Vol. 1, pp. 163-166, 1998.



Dominik Bortis (S'06-M'09) was born in Fiesch, Switzerland on 29 December 1980. He studied electrical engineering at the Swiss Federal Institute of Technology (ETH) Zurich. During his studies he majored in communication technology and automatic control engineering. In his diploma thesis he worked with Levitronix, where he designed a galvanic isolation system for analog signals. He received his M.Sc. degree in 2005, and has been a Ph.D. student

at the Power Electronic Systems Laboratory, ETH Zürich, from 2005 to 2008. Since 2008 he is working as PostDoc at the Power Electronic Systems Laboratory, ETH Zürich.



Juergen Biela (S'04-M'06) received the diploma (with honors) from the Friedrich-Alexander University in Erlangen, Germany in 2000 and the Ph.D. degree from ETH Zurich in 2005, all in electrical engineering. During his Master degree studies, he also studied at the Strathclyde University, Scotland, UK, and at the Technical University of Munich. From 2000 to 2002 he worked at the

research department of A&D Siemens. In 2002, he joined the Power Electronic Systems Laboratory (PES), ETH Zurich working towards his Ph.D. degree. After finishing his Ph.D. degree in 2005, he worked as Post-Doctoral Fellow (2006-2007) and as Senior Scientist (2008-2010) at PES. In 2007 he was a guest researcher at the Tokyo Institute of Technology, Japan. In 2010, he has been appointed associate professor for high power electronics at the ETH Zurich.



Gabriel Ortiz was born in Chuquicamata, Chile, on 13 September 1984. He studied electronics engineering at Universidad Técnica Federico Santa María, Valparaíso, Chile, joining the power electronics group early on 2007. During his Master thesis he worked with reconfiguration of regenerative and non-regenerative cascaded multilevel converters under fault condition, obtaining maximum qualification on his Thesis Examination. He received his M.Sc. degree in 2008. He has been a Ph.D. student at the Power Electronic Systems Laboratory, ETH Zürich, since 2009.



Johann W. Kolar (M'89-SM'02) studied industrial electronics at the University of Technology Vienna, Austria, where he also received the Ph.D. degree (summa cum laude). From 1984 to 2001 he was with the University of Technology in Vienna, where he was teaching and working in research in close collaboration with industry. He has proposed numerous novel converter topologies, e.g., the VIENNA Rectifier and the Three-Phase AC-AC Sparse Matrix

Converter concept. Dr. Kolar has published over 300 scientific papers in international journals and conference proceedings and has filed more than 75 patents. He was appointed Professor and Head of the Power Electronics Systems Laboratory at the ETH Zurich in 2001.